



Poly(m-Phenylene Isophthalamide)/Carbon Black Nanoparticle Composite Film as High-Temperature Electric Heater

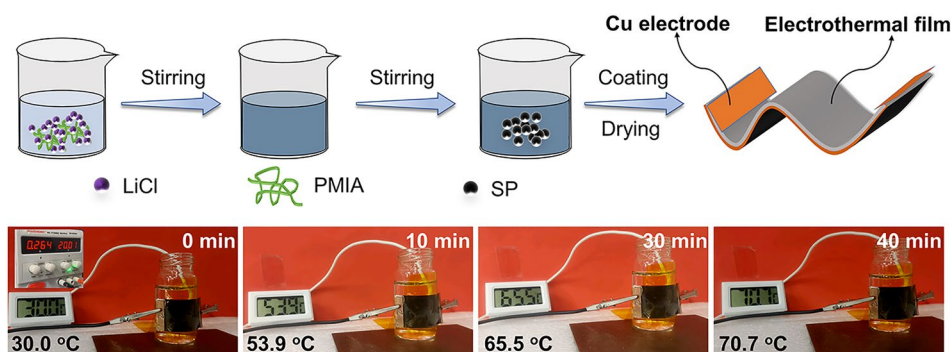
Zhongjie Shao¹ · Yaning Liu¹ · Peng Cai¹ · Qiyue Wang¹ · Zhen Xiao² · Lihui Zhang³ · Bo Tong³ · Bingjia Wang³ · Yong Zhao³ · Wenkui Zhang¹ · Yang Xia¹

Received: 30 June 2023 / Accepted: 26 April 2024
© The Minerals, Metals & Materials Society 2024

Abstract

Carbon-based conductive polymer composites have attracted wide attention as candidates for high-performance flexible electric heaters. Herein, a poly(m-phenylene isophthalamide) (PMIA)/carbon black (CB) composite is proposed as electric heating films that can successfully realize stable and safe operation at high temperatures of $> 200^{\circ}\text{C}$ under a safe voltage as low as 20 V. The conductive filler content has a significant effect on the microstructure and electrical properties of the PMIA/CB composites. An optimized CB content of 20 wt.% in the PMIA polymer matrix not only guarantees uniform spatial dispersion, but also provides sufficient and stable conductive networks. As a result, the PMIA/CB composites present high heating temperature, rapid heating ability, good heating uniformity, and excellent heating reliability. Meanwhile, taking advantage of the high thermal stability, superior mechanical strength, and excellent flame retardancy of the PMIA polymer matrix, the PMIA/CB composites exhibit superior thermal endurance and self-extinguishing capabilities, leading to significantly enhanced operating safety. This study will open new avenues for the development of high-performance electrothermal composite films for medium- to high-temperature applications.

Graphical Abstract



Keywords High-temperature electric heater · electrothermal film · carbon-polymer composites · poly(m-phenylene isophthalamide) · flame retardancy

Zhongjie Shao and Yaning Liu have contributed equally to this work.

Extended author information available on the last page of the article

Introduction

Carbon-based electrothermal films are a group of conductive polymer composites (CPCs) that represent a burgeoning class of functional materials based on the Joule thermal effect,¹ widely used in defrosters,² electrical heaters,³ thermal therapy,⁴ wearable devices,⁵ and sensors.⁶ Traditional

electrothermal materials, such the metal-based alloys and ceramic materials, have some inherent disadvantages.^{7–10} Metal-based alloys are susceptible to the induction effect when voltage is applied, leading to increased power loss and reduced efficiency in electric heat conversion.^{11–15} Ceramic electric heating materials are known for their high efficiency in electric heat conversion, as well as their corrosion and oxidation resistance.^{15–19} However, the low heating response, lack of vibration resistance, and inferior mechanical bending strength are major hindrances to the widespread applications of ceramic electric heating materials.^{20–23} Generally, CPCs consist of a polymer matrix and conductive carbon fillers, in which the polymer ensures the structural stability of the composite, and the carbon fillers are used to build a continuous conductive network to transport electrons.²⁴

However, the application of electrothermal films for high-temperature heating ($> 150^{\circ}\text{C}$) is seriously restricted due to the poor thermal stability of the polymer matrix and the low conductivity of the composite films.²⁵ In particular, the composites are prone to local heat concentration due to low thermal conductivity in the high-temperature heating state, which results in the softening of the polymer and conductive network structure failure.^{26,27} Recently, scholars have proposed a variety of strategies that have improved the upper limit of the heating temperature of electrothermal composites. Yan et al. fabricated polydimethylsiloxane (PDMS)/multi-walled carbon nanotube (MWCNT)/graphene composites with high thermal stability, which exhibited thermally durability reaching 250°C based on the highly energetic Si–O bond (108 kcal/mol).²⁸ Lee et al. reported that cellulose/MWCNT composites demonstrated composite films with well-regulated equilibrium maximum temperatures of 189°C .²⁹ Park et al. discovered that polybenzimidazole as a polymer matrix endows CPCs with remarkable mechanical strength and extraordinarily high thermal stability, resulting in a maximum stable temperature of 220°C .³⁰ Therefore, selecting polymers with high thermal stability as the matrix of electrothermal composites is a valid tool to improve the high-temperature heating performance.

Poly(m-phenylene isophthalamide) (PMIA), a synthetic polymer with good thermal stability and flame retardancy, is known as an aromatic polyamide.²⁵ It is a linear macromolecule made up of amide-bonded aromatic groups as illustrated in Fig. S1 (see supplementary Fig. S1). Accordingly, it has found increasing use across a range of engineering applications.³¹ The hydrogen bonding of the frameworks and the rigidity of the chains obviously contribute to the high glass transition temperature, measured at 274°C .³² The PMIA macromolecular chain has several stiff benzene rings, which contribute to its relatively high rigidity and outstanding mechanical properties. High energy barriers to the rotation of the sub-phenyl-amide and C–N bonds in the molecular structure prevent the PMIA molecular chain from

becoming a fully elongated chain conformation. Its unique microstructure allows it to form a unique three-dimensional intramolecular and intermolecular hydrogen bonding structure, which gives PMIA excellent heat resistance, chemical reagent resistance, mechanical, and hydrophilic properties.³³ Liu et al. fabricated PMIA/ Al_2O_3 composites to improve the thermal conductivity and mechanical properties for transformers and other electrical equipment.³⁴ PMIA has also been widely employed as a filtration membrane and lithium battery separator energy storage material in previous decades.^{35,36} However, to the best of our knowledge, there are few studies to date on PMIA as a high-temperature polymer matrix to fabricate conductive polymer composites for carbon-based electrothermal films. In light of its attractive features as discussed above, it is reasonable to conclude that PMIA is an excellent candidate for membrane material, with exceptional performance.

Herein, a series of flame-retardant PMIA/CB composite films with varying carbon black content of 10–40 wt.% were prepared using the slurry coating method, demonstrating excellent thermal stability and high safety. The morphological characteristics, thermodynamic stability, and resistivity were systematically characterized. The electrical percolation threshold of the PMIA/CB composite electrothermal films was calculated from the classical percolation theory. Importantly, PMIA based on amide bonding and intramolecular/intermolecular hydrogen bonding has significant thermal oxidation resistance up to 400°C , resulting in PMIA/CB composite electric heating film with excellent thermal stability and operational reliability.

Experimental

Raw Materials

In this work, raw materials were purchased as received without any additional purification. Poly(m-phenylene isophthalamide) (PMIA, $M_w = 200,000$) powders obtained from Yantai Taihe New Material Co. Ltd. were employed as the polymer. Carbon black (Super-P, particle size distribution = 100–150 nm) powders as conductive fillers were purchased from Shanghai Huiping New Energy Co. Ltd. Lithium chloride (LiCl, 99%) and *N,N*-dimethylformamide (DMF) were acquired from Shanghai Aladdin Biochemical Technology Co. Ltd. and Wuxi Baichuan Chemical Industry Co. Ltd, respectively.

Fabrication of PMIA/CB Composites

PMIA/CB composites were produced by a simple slurry coating technique as shown in Fig. 1a. LiCl and PMIA were dissolved into DMF and stirred continuously at 70°C

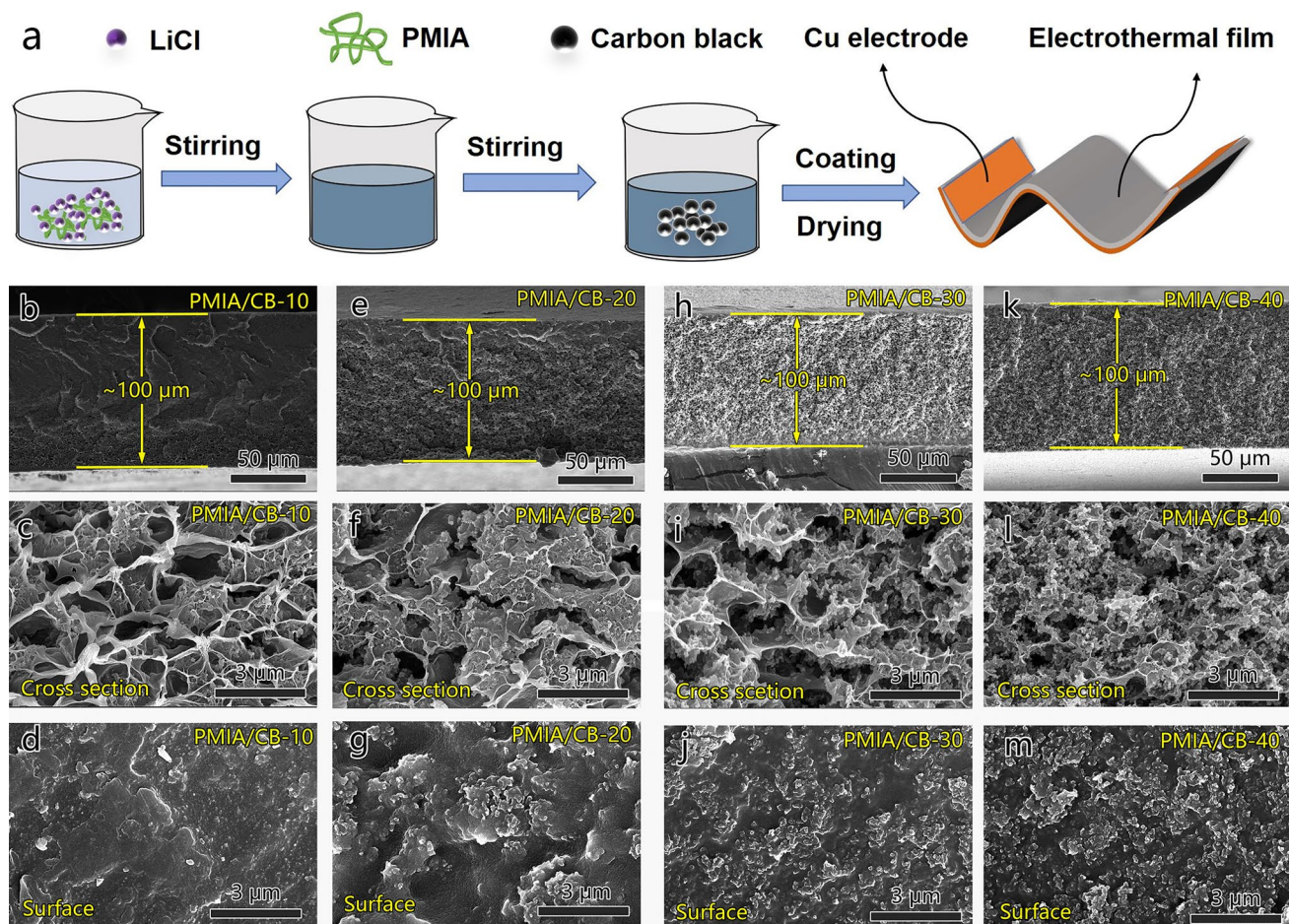


Fig. 1 (a) Diagram of the steps for synthesizing PMIA/CB composites. SEM images of PMIA/CB composites: (b–d) PMIA/CB-10, (e–g) PMIA/CB-20, (h–j) PMIA/CB-30, (k–m) PMIA/CB-40.

for 12 h. Subsequently, carbon black powders with different PMIA/CB mass ratios of 90:10, 80:20, 70:30, and 60:40 were added into the as-prepared PMIA-LiCl-DMF glue solution with vigorous stirring at 1200 r min^{-1} for 15 min (see supplementary Table SI). After that, the prepared slurry was coated onto the copper foil with a spatula and put into a vacuum vessel for 1 h to eliminate air bubbles. The samples were dried at 70°C to remove DMF solvent. Then, the obtained samples were dipped in deionized water (80°C) for 2 h to remove the residual LiCl, and this procedure was repeated twice. After cleaning, the samples were dried at 70°C for 6 h. Copper electrodes were placed on the surface of the PMIA/CB composites. The PMIA/CB composite electrothermal films were designated as PMIA/CB- x , where x represented the mass ratio of carbon black conductive particles in various PMIA/CB composite electrothermal films, PMIA/CB-10, PMIA/CB-20, PMIA/CB-30, and PMIA/CB-40, respectively. The size of the PMIA/CB composites was fixed at $20 \text{ mm}^2 \times 40 \text{ mm}^2$.

Material Characterizations and Electrothermal Measurements

Field-emission scanning electron microscopy (FE-SEM, FEI, Nova NanoSEM 450) was employed to investigate the morphology and chemical composition of the PMIA/CB composite electrothermal films. X-ray diffraction (XRD) was measured on a Rigaku Ultima IV x-ray diffractometer with $\text{Cu K}\alpha$ radiation. Fourier transform infrared (FTIR) spectra were recorded by a Nicolet 6700 spectrophotometer. Thermal stability was measured by thermogravimetric analysis (TGA, Q5000IR) from 40°C to 800°C with a heating rate of 5°C min^{-1} under N_2 atmosphere. The electrothermal properties were assessed by a homemade test system. Temperature distributions were examined using a thermal infrared (IR) camera (Fluke TiS40). The sheet resistance was evaluated by a four-point probe measurement system (M-3, JG). All the samples were actuated by a direct-current (DC) power supply (YGX-300 V-3A, Hongyou Instruments). The operating

temperatures of the electric heating films were monitored by three thermocouples in different zones.

Results and Discussion

Figure 1a depicts the optimized fabrication method for the PMIA/CB electrothermal films. The morphology and microstructure of the PMIA/CB electrothermal films were verified by SEM tests. As illustrated in Fig. 1b, e, h, and k, the cross-section SEM images of PMIA/CB-10, PMIA/CB-20, PMIA/CB-30, and PMIA/CB-40 clearly demonstrate that the thickness of the as-prepared PMIA/CB composite electrothermal films is $\sim 100 \mu\text{m}$, implying that slurry coating not only ensured the good thickness consistency of electrothermal films, but also is suitable for large-scale and low-cost manufacturing. To further investigate the interior microstructure of the PMIA/CB composite electrothermal films, high-magnification SEM images are displayed in Fig. 1c, f, i, and l. All the samples clearly exhibit a typical three-dimensional (3D) network structure, in which the intertwined PMIA (the bright white part since the PMIA polymer matrix has poor electroconductivity, resulting in a charging effect) is formed as the robust 3D skeleton, whereas the conductive particles are dispersed into the PMIA polymer matrix, endowing the 3D PMIA skeleton with spatially continuous electric conductivity. Moreover, with the increase in CB content, a small portion of CB nanoparticles fill the edge of the PMIA skeleton. Additionally, the surface morphology of the PMIA/CB samples is observed in Fig. 1d, g, j, and m. The PMIA/CB-10 sample with low CB content of 10 wt.% clearly displays a very smooth surface. There is no evident particle aggregation of CB conductive fillers. Notably, as the CB content continues to increase, the plane of the PMIA/CB samples becomes rough. Many island-like aggregates can be identified in the PMIA/CB-40 sample. In

particular, significant agglomeration of CB nanoparticles is detected in the PMIA/CB-40 sample, which may result in a negative temperature coefficient (NTC) effect,^{37–40} causing local overheating or even posing a fire hazard.

To analyze the effect of CB content on the phase structure of the PMIA/CB composite electrothermal films, the XRD patterns of the PMIA/CB samples are displayed in Fig. 2a. As for the CB conductive fillers, there are two wide diffraction peaks located at 26° and 45° , related to the (002) and (101) planes of carbon materials.^{41–43} In parallel, PMIA has only one wide characteristic diffraction peak at 24° , suggesting that PMIA is semi-crystalline in nature. Notably, when CB conductive fillers are incorporated into the PMIA polymer matrix, there is a broad diffraction peak in the range of 24° – 25° in PMIA/CB composite electrothermal films. Moreover, the broad diffraction peaks in the PMIA/CB composite electrothermal films gradually shift to 25° with increasing CB content. This result implies that excess CB nanoparticles will migrate to the edge or surface of the PMIA polymer matrix, which is in accordance with SEM results in Fig. 1. FTIR spectra are employed to investigate the surficial features of the PMIA/CB samples. As illustrated in Fig. 2b, the PMIA and PMIA/CB composite electrothermal films both show two characteristic peaks at 1410 cm^{-1} and 1647 cm^{-1} , corresponding to the stretching vibrations of the C=C and C=O groups of PMIA, respectively.⁴⁴ Meanwhile, the broad absorption peak at 3320 cm^{-1} is formed by the overlapping of the hydrogen bonds of the amide group in the carboxyl group.^{45–47} Additionally, as the amount of CB conductive fillers increases, the maximum strength of the characteristic peaks at each position gradually decreases. This situation can be ascribed to two factors. One is that the mass fraction of PMIA in the PMIA/CB samples decreases with the increased ratio of CB conductive particles, resulting in a decrease in the relative peak intensity of PMIA. On the other hand, CB conductive fillers have an even spatial

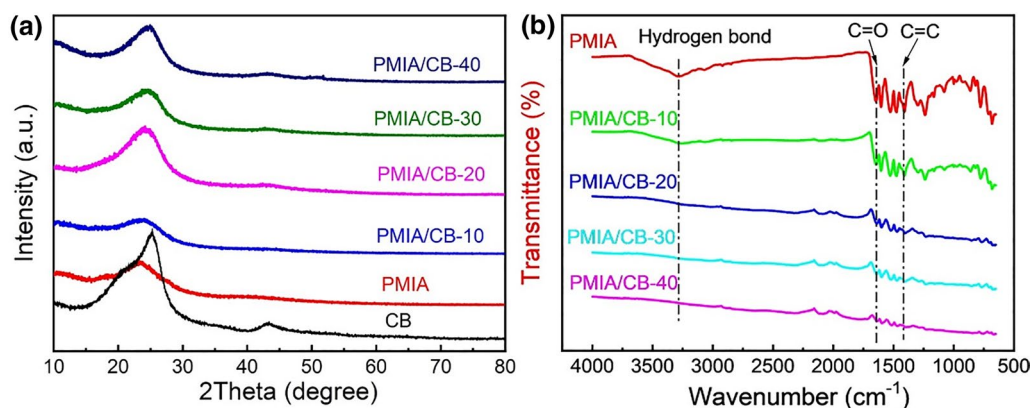


Fig. 2 (a) XRD patterns of PMIA, CB, and PMIA/CB composite electrothermal films. (b) FTIR spectra of PMIA and PMIA/CB composite electrothermal films.

distribution within PMIA, which reduces the crystallinity of PMIA by breaking the weak bonds between the molecular chain structure inside. Furthermore, the thermal stability of carbon-based polymer electrothermal composite films is crucial to the operational reliability. According to the TG results (see supplementary Fig. S2), only a slight weight loss occurs between 40°C and 100°C for all the samples, owing to the evaporation of accumulated moisture and residual water. When the temperature is increased to 400°C, a remarkable reduction in weight can be detected for all the sample, which is attributed to the breakage of amide bonds and intramolecular/intermolecular hydrogen bonds, as well as the decomposition of the PMIA macromolecule. The PMIA polymer matrix has a remarkable thermal anti-oxidative degradation before 400°C, which endows the PMIA/CB composite electrothermal films with superior thermal stability and operational reliability.

Current–voltage (I – V) curves and electric power–voltage (P – V) curves for the PMIA/CB samples are shown in Fig. 3a. The I – V curves of the PMIA/CB composites consistently demonstrate a linear relationship, implying that they obey Ohm's law ($V = I \times R$, where R is the electric resistance of the sample).^{48–51} It is noteworthy that with an increase in the CB ratio, the slope of the I – V curve becomes steeper, which is mainly due to the generation of conductive networks by increasing interrelation between the CB nanoparticles. In addition, according to the P – V curves (the inset of Fig. 3a), the electric power of the PMIA/CB samples is quadratically increased with the operation voltage, which is in conformity with the formula of $P = V^2/R$. Figure 3b displays the connection between sheet resistance and CB content. Impressively, the sheet resistance sharply decreases with increasing CB ratio from 10 wt.% to 20 wt.%. Specifically, the sheet resistance values for PMIA/CB-10 and PMIA/CB-20 are $1319 \Omega \text{ sq}^{-1}$ and $119 \Omega \text{ sq}^{-1}$, respectively. The sheet resistance

changes by an order of magnitude. However, the sheet resistance variation is prone to be stability when the CB content exceeds 20 wt.%. This variation in sheet resistance subject to the conductive filler content is typical of the percolation behavior in electric heating films. To determine the electrical percolation threshold of the PMIA/CB composite electrothermal films in this work, the classical percolation theory is adopted as described in Eq. 1:

$$\rho = C \times (\varphi - \varphi_c)^{-t}, (\varphi > \varphi_c) \quad (1)$$

where ρ , C , φ_c , φ , and t are the sheet resistivity, scaling factor, percolation threshold value, actual conductive particle ratio, and critical exponent, respectively.⁵² As shown in the graphic illustration of Fig. 3b, the straight line with $\varphi_c = 15.5$ vol.% is consistent with the testing information of the $\log \rho$ versus $\log (\varphi - \varphi_c)$ plot. The low percolation threshold value of 15.5 vol.% in the PMIA/CB composite system indicates that the conductive particles with a homogeneous distribution in PMIA build an effective conductive network that is conducive to achieving a low operating voltage.

Figure 4 presents the temperature profiles of the PMIA/CB samples over time. The electric heating properties of all the samples are clearly similar, with three regions including a fast-heating platform, steady-heating platform, and cooling platform, respectively.^{11,53,54} In the rapid-heating platform, the apparent temperature is rapidly increased to a maximum equilibrium temperature when the sample is driven by DC power with a certain applied voltage. It should be mentioned that the time for heating to 90% of the maximum steady-state equilibrium temperature (T_{max}) is indexed as the electrothermal response time, and the shorter the better.²⁵ As displayed in Fig. 4a, b, c, and d, the electrothermal response time of the PMIA/CB composite electrothermal films is less than 50 s. Finally, at the cool-down stage, the temperature quickly

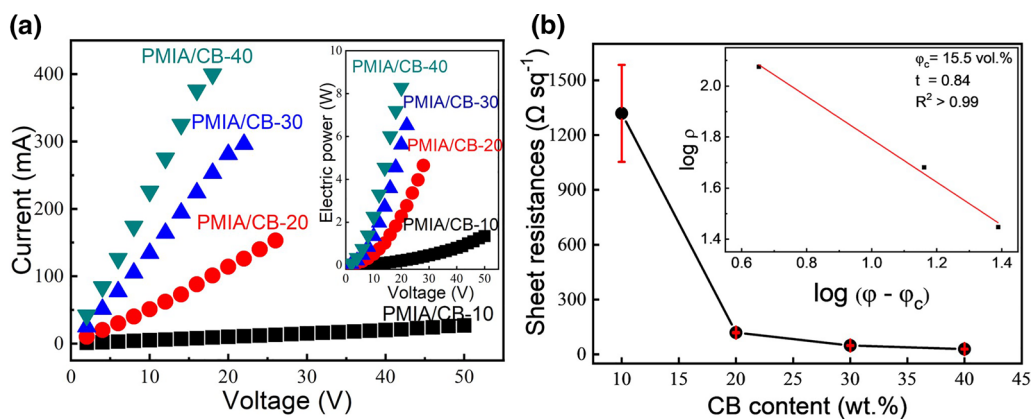


Fig. 3 (a) Current–voltage (I – V) curves of the PMIA/CB samples. The curves of the relating electric power–voltage (P – V) are shown in the photographic inset. (b) The correlation between conductive par-

ticle ratio and sheet resistance in different PMIA/CB samples. The inset is the fitting line according to the classical percolation theory.

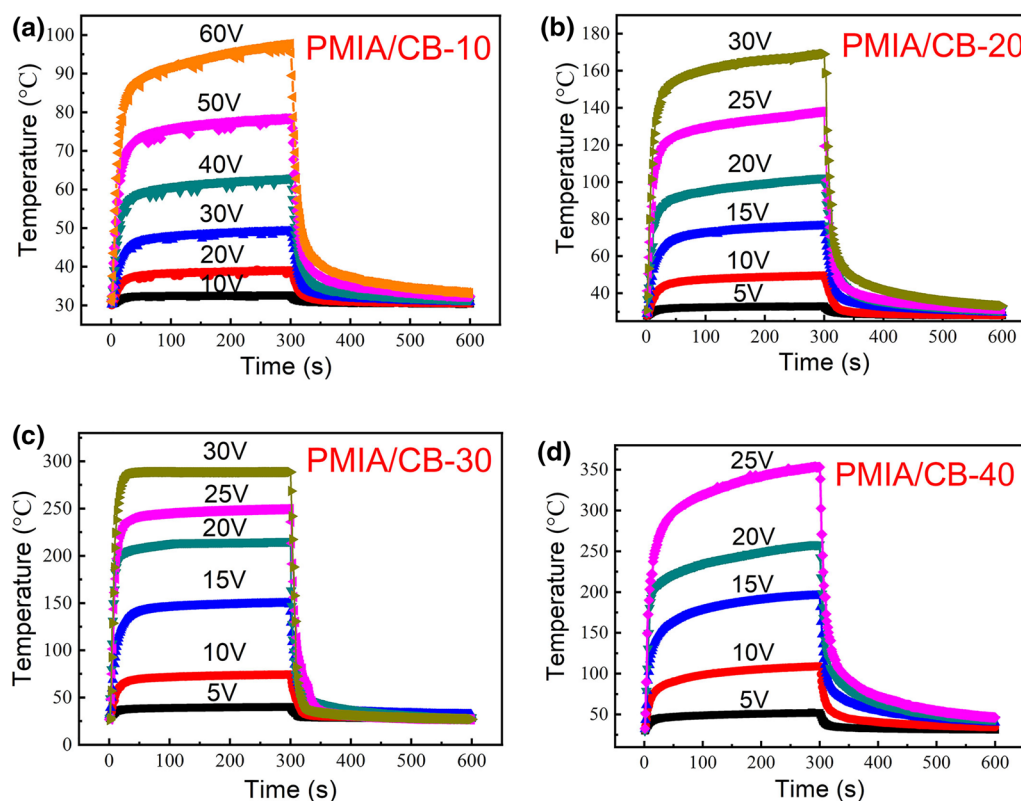


Fig. 4 Time-dependent temperature profiles of the PMIA/CB samples at different applied voltage: (a) PMIA/CB-10, (b) PMIA/CB-30, (c) PMIA/CB-30, and (d) PMIA/CB-40, respectively.

returns to room temperature within 10 s, suggesting the remarkable thermal conductivity and heat dissipation. This result indicates that the PMIA/CB samples have excellent electrothermal response ability since the highly dispersed CB conductive fillers endow the PMIA/CB composite with significantly reduced tunneling gap and enhanced electron hopping that facilitate the formation of efficient and stable conductive network. Moreover, as the applied voltage gradually rises, the T_{\max} is increased correspondingly. The T_{\max} of the PMIA/CB composite electrothermal films has a vast span from 30°C to 350°C by simply adjusting the applied voltages, which is suitable for various application scenarios. Additionally, as shown in Fig. 4d, the PMIA/CB-40 sample has the highest T_{\max} of 350°C under a voltage of 25 V. However, during the steady heating stage, the T_{\max} platform curve of the PMIA/CB-40 sample is sloping, implying that the T_{\max} could not remain stable. In contrast, the T_{\max} platform curve of the PMIA/CB-30 sample (Fig. 4c) is very flat, demonstrating the superior temperature control performance among all the samples. Finally, at the cool-down stage, the temperature quickly returns to room temperature within 10 s, suggesting the remarkable thermal conductivity and heat dissipation. In fact, Table SII (see supplementary Table SII) lists the previously reported electrothermal properties of

polymer composites. It is clear that the PMIA/CB films have the higher heating temperature and power density applying a certain voltage, which are superior than that of reported polymer composites.

Figure 5a presents the connection of steady T_{\max} and applied voltage of the PMIA/CB samples. Apparently, the steady T_{\max} of the PMIA/CB samples is quadratically increased with the higher applied voltage since the electrothermal conversion is in line with the power equation of $P = V^2/R$. To be more specific, if the sample has lower resistance and good electronic conductivity, it could deliver a higher electrothermal conversion efficiency, which will achieve a higher steady T_{\max} . Furthermore, according to the T_{\max} - P curves of the PMIA/CB samples (Fig. 5b), the samples show a linear correlation between electric power and maximum stable temperature. This characteristic allows the PMIA/CB composite electrothermal films to precisely modulate working temperature by adjusting operating conditions.

In order to verify the working reliability of the PMIA/CB samples, all the samples are evaluated by alternating heating-cooling cycling tests. As shown in Fig. 6, the PMIA/CB composite electrothermal films have a specific stable T_{\max} at the same applied voltage, which is in remarkably optimum conformance with the outcomes of the temperature profiles

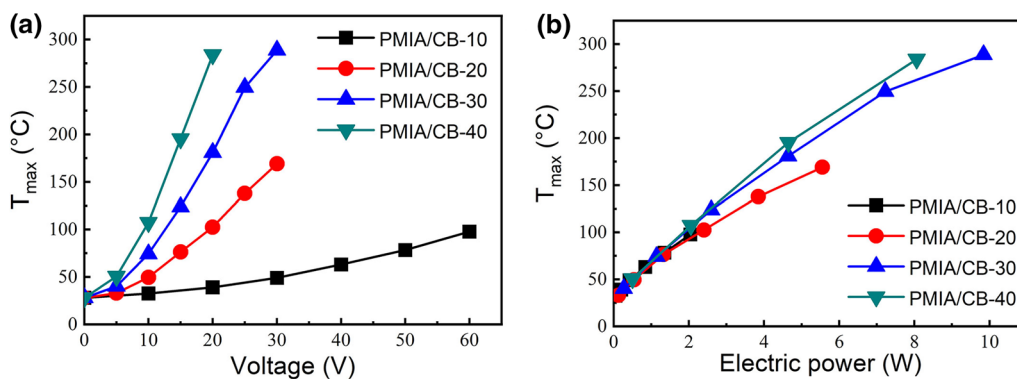


Fig. 5 (a) Maximum equilibrium temperature (T_{max}) versus applied voltage (V) plots of PMIA/CB samples. (b) Maximum equilibrium temperature (T_{max}) versus electric power (P) plots of PMIA/CB samples.

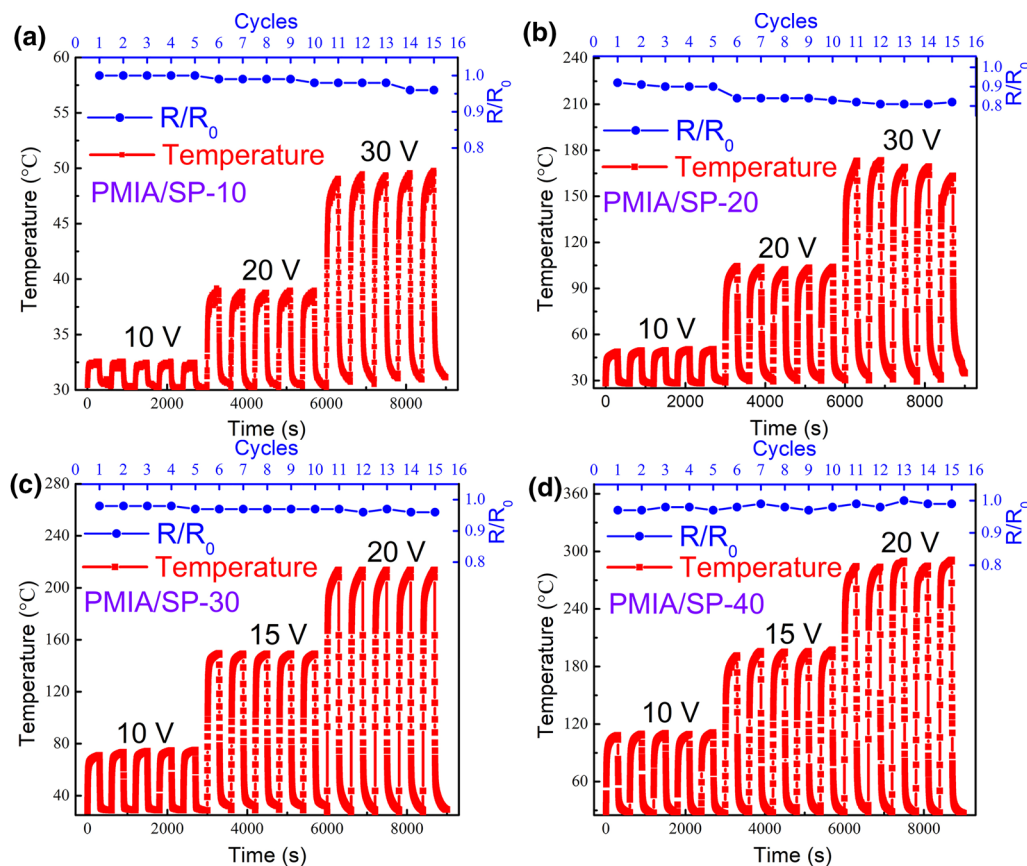


Fig. 6 Temperature responses and relative resistance changes in the PMIA/CB samples under stepwise cyclic voltage: (a) PMIA/CB-10, (b) PMIA/CB-30, (c) PMIA/CB-30, and (d) PMIA/CB-40, respectively.

over time in Fig. 4. In addition, there are no obvious changes in the T_{max} and heating–cooling behavior in repeated cycles of testing. In general, the small resistance variation implies high structural stability and long life span of the electrothermal films. Thus, the electrothermal stability of the PMIA/CB samples can be demonstrated by the volume resistance variation (R/R_0). It is noteworthy that there are conspicuous

fluctuations of the T_{max} and R/R_0 in the PMIA/CB-20 sample (Fig. 6b), suggesting that it has inferior electrothermal stability. On the contrary, the PMIA/CB-30 sample (Fig. 6c) not only maintains stable T_{max} values under various operating voltages, but also has a small volume resistance variation. Similarly, to further inspect the prolonged electrothermal reliability, the PMIA/CB-30 sample is tested under

20 V for 30 min (see supplementary Fig. S3a). Obviously, the PMIA/CB-30 sample has only a small variation of T_{\max} during the long-term heating. Meanwhile, even after a periodically repeated heating–cooling test for 20 cycles (see supplementary Fig. S3b), the T_{\max} and R/R_0 of the PMIA/CB-30 sample both remain stable. SEM images present the surface morphology and cross-sectional morphology. Impressively, Fig. S4 and Fig. S5 (see supplementary Fig. S4 and Fig. S5) clearly display the excellent oxidation resistance and remarkable electrothermal stability of the PMIA/CB-30 composite electrothermal films. The PMIA polymer matrix serves as an outstanding three-dimensional skeleton. Meanwhile, carbon black particles are tightly interconnected and uniformly scattered throughout the whole polymer matrix, forming multiple conductive networks (see supplementary Fig. S6). During the heating process, the carbon black particles will migrate slightly; however, within the electrothermal film they remain uniformly dispersed even after long-term heating–cooling cycles, demonstrating the excellent structural

stability of PMIA/CB-30. Additionally, the particle size and distribution of carbon black particles before and after heating–cooling cycles are further analyzed. As displayed in Fig. S7 (see supplementary Fig. S7), there is almost no change in the particle size of the carbon black particles. This is because the polymer wraps around the carbon black particles, protecting them from oxygen. As a result, the particles can retain their original size without oxidation, leading to the superior heating–cooling cycling reliability. Therefore, from the perspective of electrothermal response ability, maximum working temperature, and electrothermal stability and reliability, the PMIA/CB-30 sample is an ideal candidate for electrothermal material in high-temperature electric heaters.

In order to scrutinize the heating uniformity and working reliability, the PMIA/CB-30 electrothermal film is examined under different operating voltages by infrared thermography as displayed in Fig. 7a, b, c, and d. The images clearly show that the maximum equilibrium temperatures of the PMIA/CB-30 sample are 45.6°C,

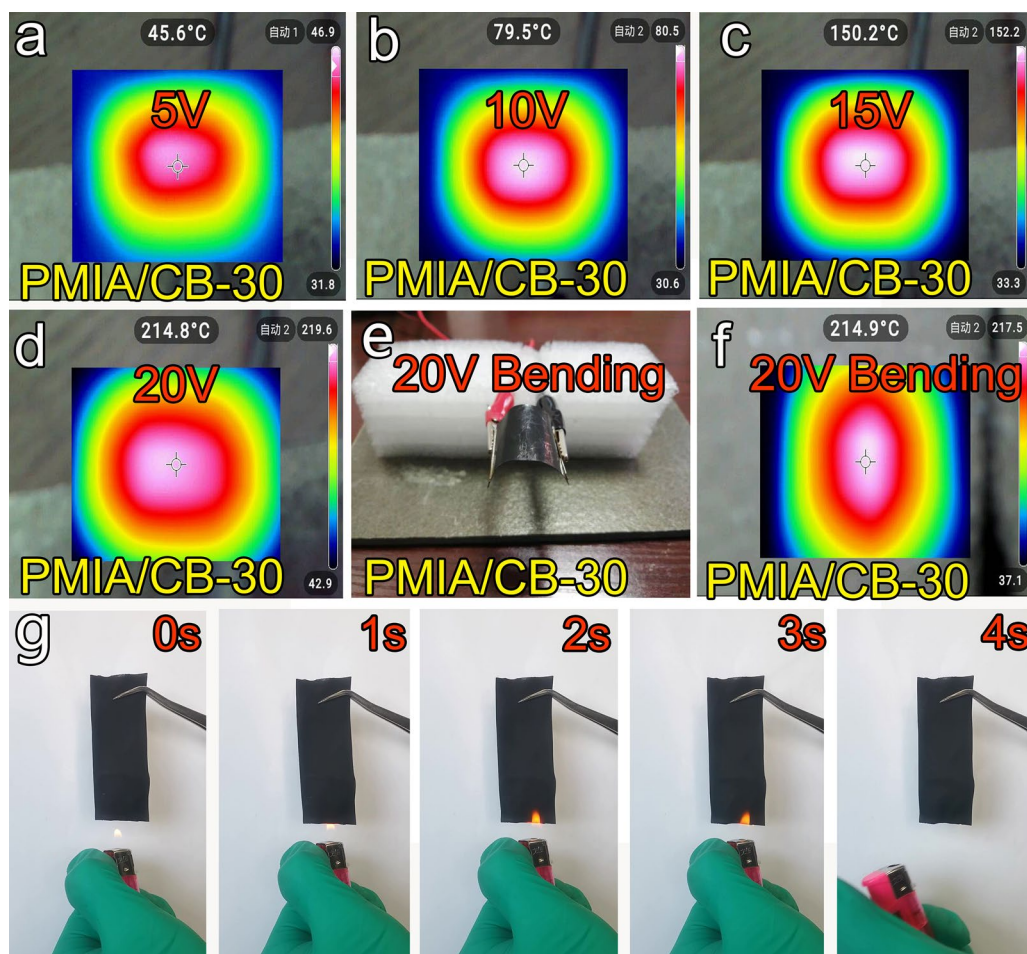


Fig. 7 (a–d) Infrared images of the PMIA/CB-30 electrothermal film under different operating voltages. (e–f) Digital image and infrared image of the PMIA/CB-30 electrothermal film working at an operat-

ing voltage of 20 V in the bent state. (g) Digital image of the PMIA/CB-30 electrothermal film ignited with flame source.

79.5°C, 150.2°C, and 214.8°C at 5 V, 10 V, 15 V, and 20 V, respectively, matching well with the results in Fig. 6c. Moreover, the surface temperature has a highly uniform distribution, which mainly originates from the homogeneous conductive network structure of the PMIA/CB-30 sample. In addition, as illustrated in Fig. 7e and f, even in the bent state, the PMIA/CB-30 sample can still achieve stable heating since no distinct surface temperature change or uneven heating phenomenon can be observed, implying the superior mechanical strength and structural stability. The flame-retardant ability of the PMIA/CB-30 sample is then assessed by a burn test to verify its safety.⁵⁵ Figure 7g clearly displays that the PMIA/CB-30 sample has outstanding self-extinguishing ability even when igniting with a lighter for 3 s. Obviously, the PMIA/CB-30 sample as an electric heater has preferable flame retardancy, which could guarantee safe operation when it is used in household appliances.

On the basis of the aforementioned excellent electrothermal performance, the PMIA/CB-30 sample is employed as a portable electric heater. In this work, as illustrated in Fig. 8, the PMIA/CB-30 electrothermal film is attached to the side of a glass bottle for heating water. Powered by a 20 V power supply, the temperature of water in the glass bottle rises rapidly from 30°C to 53.9°C within 10 min. After 30 min, the water temperature reaches 65.5°C. Finally, the water temperature

stabilizes at 70.7°C. This result demonstrates that the rationally designed PMIA/CB-30 electrothermal film has great potential in various household appliances.

Conclusion

In summary, the rationally designed PMIA/CB composite electrothermal films with 100 µm thickness are manufactured by a slurry coating method for the medium- to high-temperature applications. The relationship between microstructure and electrothermal properties is systematically investigated. The PMIA/CB samples have a rapid electrothermal response time of less than 50 s, which is substantially faster than most previously reported electric heaters. In particular, the PMIA/CB-30 sample not only retains an extremely high maximum heating temperature (>200°C) with a small volume resistance variation, but also exhibits outstanding electrothermal reliability during prolonged heating-cooling tests. Moreover, the PMIA/CB composite electrothermal films have superior self-extinguishing ability within 4 s during the burn test, demonstrating excellent flame retardancy and safety. Overall, it is expected that these rationally designed PMIA/CB composite films will significantly push the boundary of electric heating elements for the practical application in medium- to high-temperature household appliances.

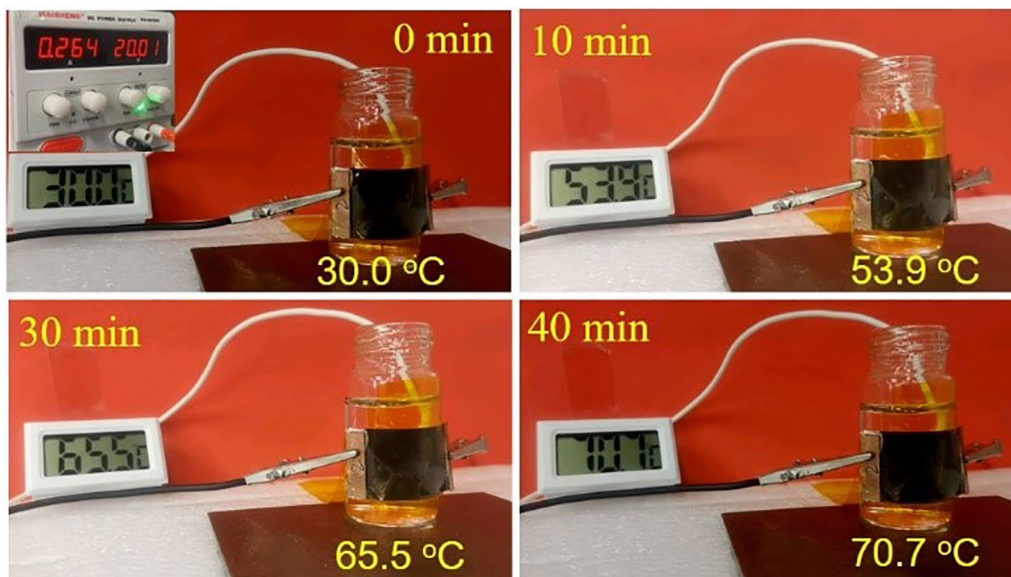


Fig. 8 Digital images of the PMIA/CB-30 electrothermal film as an electric heater for heating water.

Supplementary Information The online version contains supplementary material available at <https://doi.org/10.1007/s11664-024-11147-0>.

Acknowledgments This work was supported by the “Research and application on efficient deicing and anti-icing technologies for wind turbine blades” of the science and technology project of Huaneng Group Co., Ltd. (HNKJ22-H101), National Natural Science Foundation of China (22279116), Natural Science Foundation of Zhejiang Province (LY21E020005), China Postdoctoral Science Foundation (2020M671785 and 2020T130597), and Fundamental Research Funds for the Provincial Universities of Zhejiang (2022YW54).

Conflict of interest The authors declare that they have no conflict of interest.

References


- D. Sui, Y. Huang, L. Huang, J.J. Liang, Y.F. Ma, and Y.S. Chen, Flexible and transparent electrothermal film heaters based on graphene materials. *Small* 7, 3186 (2011).
- Y. Xia, P. Cai, Y. Liu, J. Zhu, R. Guo, W. Zhang, Y. Gan, H. Huang, J. Zhang, C. Liang, X. He, and Z. Xiao, A low-cost and high-efficiency electrothermal composite film composed of hybrid conductivity fillers and polymer blends matrix for high-performance plate heater. *J. Electron. Mater.* 50, 3084 (2021).
- H. Souri, S.J. Yu, H. Yeo, M. Goh, J.-Y. Hwang, S.M. Kim, B.-C. Ku, Y.G. Jeong, and N.-H. You, A facile method for transparent carbon nanosheets heater based on polyimide. *RSC Adv.* 6, 52509 (2016).
- H. Li, Z. Li, N. Li, X. Zhu, Y. Zhang, L. Sun, R. Wang, J. Zhang, Z. Yang, H. Yi, X. Xu, and H. Lan, 3D printed high performance silver mesh for transparent glass heaters through liquid sacrificial substrate electric-field-driven jet. *Small* 18, 2107811 (2022).
- M. Zhang, C. Wang, X. Liang, Z. Yin, K. Xia, H. Wang, M. Jian, and Y. Zhang, Weft-knitted fabric for a highly stretchable and low-voltage wearable heater. *Adv. Electron. Mater.* 3, 1700193 (2017).
- J. Sun, J. Zhuang, J. Shi, S. Kormakov, Y. Liu, Z. Yang, and D. Wu, Highly elastic and ultrathin nanopaper-based nanocomposites with superior electric and thermal characteristics. *J. Mater. Sci.* 54, 8436 (2019).
- M.V. Zdorovets, A.L. Kozlovskiy, D.I. Shlimas, and D.B. Borgekov, Phase transformations in FeCo-Fe₂CoO₄/Co₃O₄-spinel nanostructures as a result of thermal annealing and their practical application. *J. Mater. Sci. Mater. Electron.* 32, 16694 (2021).
- F.G. Agayev, S.V. Trukhanov, A.V. Trukhanov, S.H. Jabarov, G.S. Ayyubova, M.N. Mirzayev, E.L. Trukhanova, D.A. Vinnik, A.L. Kozlovskiy, M.V. Zdorovets, and A.S. Sombra, Study of structural features and thermal properties of barium hexaferrite upon indium doping. *J. Therm. Anal. Calorim.* 147(24), 14107 (2022).
- S.V. Trukhanov, A.V. Trukhanov, V.G. Kostishyn, N.S. Zabeivorota, L.V. Panina, A.V. Trukhanov, V.A. Turchenko, E.L. Trukhanova, V.V. Oleynik, O.S. Yakovenko, and L.Y. Matzui, High-frequency absorption properties of gallium weakly doped barium hexaferrites. *Philos. Mag.* 99(5), 585 (2019).
- D.A. Vinnik, AYu. Starikov, V.E. Zhivulin, K.A. Astapovich, V.A. Turchenko, T.I. Zubar, S.V. Trukhanov, J. Kohout, T. Kmječ, O. Yakovenko, L. Matzui, A.S.B. Sombra, D. Zhou, R.B. Jotania, C. Singh, Y. Yang, and A.V. Trukhanov, Changes in structure, magnetization and resistivity of BaFe_{12-x}Ti_xO₁₉. *ACS Appl. Electron. Mater.* 3, 1583 (2021).
- K.K. Kadyrzhanov, D.I. Shlimas, A.L. Kozlovskiy, and M.V. Zdorovets, Research of the shielding effect and radiation resistance of composite CuBi₂O₄ films as well as their practical applications. *J. Mater. Sci. Mater. Electron.* 31, 11729 (2020).
- R.E. El-Shater, H. El Shimy, S.A. Saafan, M.A. Darwish, D. Zhou, K.C.B. Naidu, M.U. Khandaker, Z. Mahmoud, A.V. Trukhanov, S.V. Trukhanov, and F. Fakhry, Fabrication of doped ferrites and exploration of its structure and magnetic behavior. *Mater. Adv.* 4, 2794 (2023).
- A.L. Kozlovskiy, and M.V. Zdorovets, Synthesis, structural, strength and corrosion properties of thin films of the type CuX (X= Bi, Mg, Ni). *J. Mater. Sci. Mater. Electron.* 30(30), 11819 (2019).
- T. Zubar, V. Fedosyuk, D. Tishkevich, O. Kanafyev, K. Astapovich, A. Kozlovskiy, M. Zdorovets, D. Vinnik, S. Gudkova, E. Kaniukov, A.S.B. Sombra, D. Zhou, R.B. Jotania, C. Singh, S. Trukhanov, and A. Trukhanov, The effect of heat treatment on the microstructure and mechanical properties of 2D nanostructured Au/NiFe system. *Nanomaterials* 10, 1077 (2020).
- A.V. Trukhanov, N.A. Algarou, Y. Slimani, M.A. Almessiere, A. Baykal, D.I. Tishkevich, D.A. Vinnik, M.G. Vakhitov, D.S. Klygach, M.V. Silibin, T.I. Zubar, and S.V. Trukhanov, Peculiarities of the microwave properties of hard-soft functional composites SrTb_{0.01}Tm_{0.01}Fe_{11.98}O₁₉-AFe₂O₄ (A = Co, Ni, Zn, Cu and Mn). *RSC Adv.* 10, 32638 (2020).
- A.L. Kozlovskiy, and M.V. Zdorovets, Effect of doping of Ce^{4+/3+} on optical, strength and shielding properties of (05-x)TeO_{2-0.25}MoO_{-0.25}Bi₂O_{3-x}CeO₂ glasses. *Mater. Chem. Phys.* 263, 124444 (2021).
- O.S. Yakovenko, LYu. Matzui, L.L. Vovchenko, V.V. Oliynyk, V.V. Zagorodnii, S.V. Trukhanov, and A.V. Trukhanov, Electromagnetic properties of carbon nanotubes / BaFe_{12-x}Ga_xO₁₉ / epoxy composites with random and oriented filler distribution. *Nanomaterials* 11, 2873 (2021).
- A.V. Trukhanov, D.I. Tishkevich, S.V. Podgornaya, EYu. Kaniukov, M.A. Darwish, T.I. Zubar, A.V. Timofeev, E.L. Trukhanova, V.G. Kostishyn, and S.V. Trukhanov, Impact of the nanocarbon on magnetic and electrodynamic characteristics of the ferrite/polymer composites. *Nanomaterials* 12, 868 (2022).
- S.V. Trukhanov, D.P. Kozlenko, and A.V. Trukhanov, High hydrostatic pressure effect on magnetic state of anion-deficient La_{0.70}Sr_{0.30}MnO_x perovskite manganites. *J. Magn. Magn. Mater.* 320, e88 (2008).
- Z. Xiao, C. Sheng, Y. Xia, X. Yu, C. Liang, H. Huang, Y. Gan, J. Zhang, and W. Zhang, Electrical heating behavior of flexible thermoplastic polyurethane/Super-P nanoparticle composite films for advanced wearable heaters. *J. Ind. Eng. Chem.* 71, 293 (2019).
- A. Kozlovskiy, K. Egizbek, M.V. Zdorovets, M. Ibragimova, A. Shumskaya, A.A. Rogachev, Z.V. Ignatovich, and K. Kadyrzhanov, Evaluation of the efficiency of detection and capture of manganese in aqueous solutions of FeCeO_x nanocomposites doped with Nb₂O₅. *Sensors* 20, 4851 (2020).
- S.V. Trukhanov, I.O. Troyanchuk, V.V. Fedotova, V.A. Ryzhov, A. Maignan, D. Flahaut, H. Szymczak, and R. Szymczak, Magnetic properties of the nonstoichiometric Sr-doped manganites. *Phys. Stat. Solidi* 242, 1123 (2005).
- A.L. Kozlovskiy, and M.V. Zdorovets, Study of hydrogenation processes in radiation-resistant nitride ceramics. *J. Mater. Sci. Mater. Electron.* 31, 11227 (2020).
- N.B. Kiremitler, A. Esidir, Z. Gozutok, A.T. Ozdemir, and M.S. Onses, Rapid fabrication of high-performance transparent electrodes by electrospinning of reactive silver ink containing nanofibers. *J. Ind. Eng. Chem.* 95, 109 (2021).
- S. Zhu, C.-W. Lou, S. Zhang, N. Wang, J. Li, Y. Feng, R. He, C. Xu, and J.-H. Lin, Clean surface additive manufacturing of aramid paper-based electrically heated devices for medical therapy application. *Surf. Inter.* 29, 101689 (2022).

26. Y.Q. Li, W.B. Zhu, X.G. Yu, P. Huang, S.Y. Fu, N. Hu, and K. Liao, Multifunctional wearable device based on flexible and conductive carbon sponge/polydimethylsiloxane composite. *ACS Appl. Mater. Inter.* 8, 33189 (2016).
27. Z. Zeng, N. Wu, J. Wei, Y. Yang, T. Wu, B. Li, S.B. Hauser, W. Yang, J. Liu, and S. Zhao, Porous and ultra-flexible crosslinked MXene/polyimide composites for multifunctional electromagnetic interference shielding. *Nano-Micro. Lett.* 14, 59 (2022).
28. D. Wang, D.W. Li, M. Zhao, Y. Xu, and Q.F. Wei, Multifunctional wearable smart device based on conductive reduced graphene oxide/polyester fabric. *Appl. Surf. Sci.* 454, 218 (2018).
29. S. Zhao, P.-X. Zheng, H.-L. Cong, and A.-L. Wan, Facile fabrication of flexible strain sensors with AgNPs-decorated CNTs based on nylon/PU fabrics through polydopamine templates. *Appl. Surf. Sci.* 558, 149931 (2021).
30. L. Paredes-Madrid, C.A. Palacio, A. Matute, and C.A. Parra Vargas, Underlying physics of conductive polymer composites and force sensing resistors (FSRs) under static loading conditions. *Sensors* 17, 2108 (2017).
31. J. Luo, S. Gao, H. Luo, L. Wang, X. Huang, Z. Guo, X. Lai, L. Lin, R.K.Y. Li, and J. Gao, Superhydrophobic and breathable smart MXene-based textile for multifunctional wearable sensing electronics. *Chem. Eng. J.* 406, 126898 (2021).
32. C. Tan, Z. Dong, Y. Li, H. Zhao, X. Huang, Z. Zhou, J.-W. Jiang, Y.-Z. Long, P. Jiang, T.-Y. Zhang, and B. Sun, A high performance wearable strain sensor with advanced thermal management for motion monitoring. *Nat. Commun.* 11, 3530 (2020).
33. M. Safarpour, V. Vatanpour, and A. Khataee, Preparation and characterization of graphene oxide/TiO₂ blended PES nanofiltration membrane with improved antifouling and separation performance. *Desalination* 393, 65 (2016).
34. Y. Zhang, Z. Ma, K. Ruan, and J. Gu, Multifunctional Ti₃C₂T_x-(Fe₃O₄/polyimide composite films with Janus structure for outstanding electromagnetic interference shielding and superior visual thermal management. *Nano Res.* 15, 5601 (2022).
35. T. Wang, X.-P. He, Y. Li, and J.-D. Li, Novel poly(piperazineamide) (PA) nanofiltration membrane based poly(m-phenylene isophthalamide) (PMIA) hollow fiber substrate for treatment of dye solutions. *Chem. Eng. J.* 351, 1013 (2018).
36. H. Zhang, Y. Zhang, T. Xu, A.-E. John, Y. Li, W. Li, and B. Zhu, Poly(m-phenylene isophthalamide) separator for improving the heat resistance and power density of lithium-ion batteries. *J. Power. Sour.* 329, 8 (2016).
37. J. Li, H. Sun, S.-Q. Yi, K.-K. Zou, D. Zhang, G.-J. Zhong, D.-X. Yan, and Z.-M. Li, Flexible polydimethylsiloxane composite with multi-scale conductive network for ultra-strong electromagnetic interference protection. *Nano-Micro. Lett.* 15, 15 (2023).
38. J. Xu, X. Zhang, Z. Zhao, H. Hu, B. Li, C. Zhu, X. Zhang, and Y. Chen, Lightweight, fire-retardant, and anti-compressed honeycombed-like carbon aerogels for thermal management and high-efficiency electromagnetic absorbing properties. *Small* 17, 2102032 (2021).
39. X.D. Pan, D.J. Guo, and H. He, Novel conductive polymer composites based on CNTs/CNFs bridged liquid metal. *J. Phys. D Appl. Phys.* 54, 085401 (2021).
40. N.A.M. Radzuan, M.Y. Zakaria, A.B. Sulong, and J. Sahari, The effect of milled carbon fibre filler on electrical conductivity in highly conductive polymer composites. *Compos. Part B-Eng.* 110, 153 (2017).
41. Z. Xiao, R. Guo, X.P. He, Y.P. Gan, J. Zhang, H. Huang, W.K. Zhang, B.J. Wang, Y. Han, and Y. Xia, Polybenzimidazole/conductive carbon black composite driven at low voltage for high-temperature heaters. *J. Electron. Mater.* 51, 2652 (2022).
42. J. Yan, and Y.G. Jeong, Synergistic effect of hybrid carbon fillers on electric heating behavior of flexible polydimethylsiloxane-based composite films. *Compos. Sci. Technol.* 106, 134 (2015).
43. T.-W. Lee, and Y.G. Jeong, Regenerated cellulose/multiwalled carbon nanotube composite films with efficient electric heating performance. *Carbohydr. Polym.* 133, 456 (2015).
44. J. Park, and Y.G. Jeong, Investigation of microstructure and electric heating behavior of hybrid polymer composite films based on thermally stable polybenzimidazole and multiwalled carbon nanotube. *Polymer* 59, 102 (2015).
45. J. Liu, J. Wang, L. Zhu, X. Chen, Q. Ma, L. Wang, X. Wang, and W. Yan, A high-safety and multifunctional MOFs modified aramid nanofiber separator for lithium-sulfur batteries. *Chem. Eng. J.* 411, 128540 (2021).
46. C.W. Zhao, B. Yang, J.L. Han, Y.Y. Meng, L. Yu, D.Y. Hou, J. Wang, Y. Zhao, Y.H. Zhai, S.G. Wang, and X.F. Sun, Preparation of carboxylic multiwalled-carbon-nanotube-modified poly(m-phenylene isophthalamide) hollow fiber nanofiltration membranes with improved performance and application for dye removal. *Appl. Surf. Sci.* 453, 502 (2018).
47. H. Zhang, X. Du, J. Liu, Y.H. Bai, J. Nie, J. Tan, Z. He, M. Zhang, J. Li, and Y. Ni, A novel and effective approach to enhance the interfacial interactions of meta-aramid fibers. *J. Ind. Eng. Chem.* 120, 244 (2023).
48. Y.-N. Liu, Z. Xiao, W.-K. Zhang, J. Zhang, H. Huang, Y.-P. Gan, X.-P. He, G.G. Kumar, and Y. Xia, Poly(m-phenylene isophthalamide)-reinforced polyethylene oxide composite electrolyte with high mechanical strength and thermostability for all-solid-state lithium metal batteries. *Rare Met.* 41, 3762 (2022).
49. F. Wang, K. Zhang, W. Liang, Z. Wang, and B. Yang, Experimental and analytical studies on the flexible, low-voltage electrothermal film based on the multi-walled carbon nanotube/polymer nanocomposite. *Nanotechnology* 30, 065704 (2019).
50. C.-E. Lin, J. Wang, M.-Y. Zhou, B.-K. Zhu, L.-P. Zhu, and C.-J. Gao, Poly(m-phenylene isophthalamide) (PMIA): A potential polymer for breaking through the selectivity-permeability trade-off for ultrafiltration membranes. *J. Membrane. Sci.* 518, 72 (2016).
51. C.-E. Lin, L.-F. Fang, S.Y. Du, Z.-K. Yao, and B.-K. Zhu, A novel positively charged nanofiltration membrane formed via simultaneous cross-linking/quaternization of poly(m-phenylene 5 isophthalamide)/polyethyleneimine blend membrane. *Sep. Purif. Technol.* 212, 101 (2019).
52. Y. Liu, Z. Xiao, W. Zhang, H. Huang, J. Zhang, Y. Gan, X. He, B. Wang, Y. Han, and Y. Xia, Glass fiber reinforced graphite/carbon black@PES composite films for high-temperature electric heaters. *J. Ind. Eng. Chem.* 107, 401 (2022).
53. J. Sierchula, M.P. Dabrowski, and K. Czerski, Negative temperature coefficients of reactivity for metallic fuel Dual Fluid Reactor. *Prog. Nucl. Energ.* 146, 104126 (2022).
54. Q. Liu, and J.J. Richards, Rheo-electric measurements of carbon black suspensions containing polyvinylidene difluoride in N-methyl-2-pyrrolidone. *J. Rheol.* 67, 647 (2023).
55. Y.M. Yu, Y. Zhang, L.D. Xi, Z.N. Zhao, S.Q. Huo, G.B. Huo, Z.P. Huang, Z.P. Fang, and P.A. Song, Interface nanoengineering of a core-shell structured biobased fire retardant for fire-retarding polylactide with enhanced toughness and UV protection. *J. Clean. Prod.* 336, 130372 (2022).

Publisher's Note Springer Nature remains neutral with regard to jurisdictional claims in published maps and institutional affiliations.

Springer Nature or its licensor (e.g. a society or other partner) holds exclusive rights to this article under a publishing agreement with the author(s) or other rightsholder(s); author self-archiving of the accepted manuscript version of this article is solely governed by the terms of such publishing agreement and applicable law.

Authors and Affiliations

Zhongjie Shao¹ · Yaning Liu¹ · Peng Cai¹ · Qiyue Wang¹ · Zhen Xiao² · Lihui Zhang³ · Bo Tong³ · Bingjia Wang³ · Yong Zhao³ · Wenkui Zhang¹ · Yang Xia¹ 

✉ Zhen Xiao
xiaozhen@cjlu.edu.cn

✉ Yang Xia
nanoshine@zjut.edu.cn

¹ College of Materials Science and Engineering, Zhejiang University of Technology, Hangzhou 310014, China

² Key Laboratory of Rare Earth Optoelectronic Materials and Devices of Zhejiang Province, Institute of Optoelectronic Materials and Devices, China Jiliang University, Hangzhou 310018, China

³ Xi'an Thermal Power Research Institute Co., Ltd, Xi'an 710054, China